Synthesis, Photophysical characterization and dye adsorption behavior in unsymmetrical squaraine dyes with varying anchoring groups

Ajendra Kumar Vats, Anusha Pradhan, Shuzi Hayase, Shyam S Pandey

Graduate School of Life Science and System Engineering, Kyushu Institute of Technology, 2-4 Hibikino, Wakamatsu, Kitakyushu, 808-0196, Japan.

Abstract

Four newly designed unsymmetrical squaraine dyes bearing different functional groups for their anchoring on the surface of mesoporous TiO_2 were successfully synthesized aiming towards development of far-red sensitizers for dye-sensitized solar cells (DSSCs). The synthesized dyes were characterized by ^1H NMR, fast ion bombardment mass, and subjected to photophysical investigations by electronic absorption/fluorescence emission spectroscopy and cyclic voltammetry. These dyes exhibited excellent solubility in a number of common organic solvents. Adsorption behavior of these dyes on the thin films of mesoporous TiO_2 was investigated in detail and results indicated that rate of dye adsorption follows the order $–COOH>-PO_3H_2>OH>SO_3H$. At the same time, dye desorption studies demonstrated that stability of adsorbed dyes on the mesoporous TiO_2 follows the order $-PO_3H_2>>-OH>-COOH>SO_3H$. Further, implication of the nature of anchoring groups of dye molecules upon the energy levels of their highest occupied molecular orbital and lowest unoccupied molecular orbital was evaluated by both of the combined theoretical and experimental approaches. In spite of enhanced dye loading, very high binding strength and favorable energetic cascade, SQ-143 bearing Phosphonic acid exhibited hampered

photovoltaic performance as compared to that of SQ-138 with carboxylic acid anchoring group. Amongst various sensitizers used for present investigation, SQ-138 exhibited best photovoltaic performance having short-circuit current density, open circuit voltage and fill factor of 12.49 mA/cm^2, 0.60 V, and 0.53, respectively, leading to power conversion efficiency of 4.07 % after simulated solar irradiation.

Introduction

Increasing standard of life with increasing world population has urged for the design and development of novel organic photofunctional organic materials as the integral component of various electronic devices like field effect transistors [1-2], sensors [3-4], and solar cells [5-6] etc. To circumvent futuristic huge energy demands, solar cells has got enormous attention and amongst them dye sensitized solar cells (DSSCs) [7], where logical design of new functional molecules along with diverse synthetic strategies are the overwhelming topic these days. Functional dye molecules can be considered as the "heart of DSSCs" considering its prevalent role as sensitizer in the photon harvesting [8]. The first dye reported for DSSCs was based on the ruthenium complex, which had showcased a good performance with 7% efficiency [5]. However, the main drawback of metal-based dyes is the difficulty in synthesis, purification and use of rare metals. To circumvent this, effort has been switched to the development of metal free dyes owing to the fine-tuning of the energetics, ease of synthesis and less toxicity [9]. Dyes with extended π-conjugation based on triarylamine [10-11], carbazole [12-13], indoline etc., stand as the model for metal free dyes exhibiting efficient photon harvesting in the visible spectral window leaving the near infrared (NIR) region void. Thus recent hot topic of research is the strategy for the design of NIR absorbing dyes in order to achieve the panchromatic photon harvesting in combination with huge available candidates of visible dyes developed so far [14]. In an interesting and recent report on the development of highly efficient dye sensitizer with an efficiency of nearly 14 % in spite of only visible light harvesting provides a good hope for further enhancement in the overall power conversion efficiency by implementation of the NIR dyes [15]. Organic dyes face a paramount challenge for its stability, which had to be pondered upon effusively for highly efficient DSSCs. Amongst the candidature for NIR dyes, squaraine dyes are one of potential class of dyes owing to

their intense light absorption and tuning of the absorption window from NIR to IR wavelength region with very high molar extinction coefficient [16]. Squaraine dyes bear a planar Donor-Acceptor-Donor zwitterionic molecular framework with the electron deficient central Huckel ring (cyclobutadione), where the charge is delocalized over the whole molecule [17].

In DSSCs, dye molecules are attached to the semiconductor surface (generally TiO_2) by their anchoring group [18]. It is, therefore, highly desired to have a suitable anchoring group to graft them optimally onto the TiO_2 in order to have better electronic coupling and facile electron injection. It has been found that the electron-transfer efficiency at the dye–semiconductor interface is highly dependent on many factors and one of them being, how the chromophore is attached to the semiconductor surface [19]. The strong interaction of the anchoring group onto the TiO_2 would also contribute to the better stability of the dyes and the DSSC as a whole, which is a major hurdle for commercialisation. Although numerous studies on the anchoring group of sensitizers have been reported but carboxylic acid and cyanoacrylic acid anchoring has received considerable attention in terms of improved photoconversion efficiency [20]. As dye-TiO_2 interface plays a crucial role and to achieve more grip over electron transfer reactions across it, other robust anchoring groups like phosphonic acid, silatrane, salicylate, sulphonic acid, and acetylacetonate derivatives have been investigated in the past [21-23]. Amongst them, the phosphonate group has proved itself as an alternative to the carboxylate moiety due to its increased binding affinity for TiO_2 yet they suffer from retarded electron injection [24]. However, it has not been implemented on NIR dyes and also proper design of it may eradicate the injection problems too. Thus a satiable NIR dye design having anchoring group with strong binding affinity would pave the way for stable and efficient DSSC. In an utter interesting report by Kakiage et al, a silyl anchoring group based dye

showcased a strong binding affinity with TiO_2, which in turn has enhanced the stability of dye as well as overall device with an appreciable efficiency [25].

In this article, we have synthesized a series of unsymmetrical squaraine dyes having intense blue colo, strong light absorption and emisson in the far-red wavelength region. To address the stability issues, we have introduced four different anchoring groups keeping the main dye molecular framework the same in order to discuss the explict behavior of the anchoring groups. To accomplish this, unsymmetrical squaraine dyes with varying anchoring groups like –COOH (SQ-138), -OH (SQ-141) -SO$_3$H group (SQ-142) and -PO$_3$H$_2$ (SQ-143) with molecular structure as shown in the Fig. 1 have been designed, synthesized and subjected to photophysical investigations. Apart from the exploring the role of anchoring groups on dye adsorption/desorption behavior on the mesoporous TiO_2, the energetics of the dyes with respect to the conduction band (CB) of the TiO_2 and the redox potential of the iodine based electrolyte have also been investigated to compare their suitability as sensitizer. Thus we have investigated the energy of their highest occupied moleclar orbital (HOMO) and lowest unoccupied molecular orbital (LUMO) by both of the theoretical (quantum chemical) and experimental techniques. Apart from this, adsorption behaviour of these dyes on to the surface of thin films of mesoporous TiO_2 and their binding sterngth and implicaion of nature of anchoring groups on the photovoltaic behavior have also been investigated in detail.

2. Experimental

2.1 Materials and Methods

Prior to the synthesis of the dyes, their molecular structure was subjected to theoretical quantum chemical calculations using G09 software [26]. Calculation have been done using 6-311G basis

set, B3PW91 hybrid functional and time-dependent density functional theory (TD-DFT) in order to elucidate the optimized structure and calculate the energy of their HOMO and LUMO along with electronic absorption spectra. All of the chemicals were of analytical grade and used as it is without any further purifications. Synthesis was monitored by thin layer chromatography (TLC) using 60G F25 TLC plate as well as by high-performance liquid chromatography (HPLC). Synthesized intermediates and final dyes were then subjected to Matrix-Assisted Laser Desorption and Ionization (MALDI)-Time-of-Flight (TOF)-mass or Fast Ion Bombardment (FAB)-mass spectrometry in the positive ion-monitoring mode to confirm the structural identity. Finally, nuclear magnetic resonance (NMR) spectra of the final dyes dissolved in deuterated chloroform were recorded with NMR spectrometer (JEOL, 500 MHz) for the final structural verification. Electronic absorption spectra of the dyes were taken in both of the solution as well as solid state using UV-visible-NIR spectrometer (JASCO V550). Fluorescence emission spectra of the dyes were measured with a fluorescence spectrometer (JASCO FP-6600). HOMO energy level of the dyes was determined using photoelectron yield spectroscopy (Bunko Keiki Co. Ltd., model KV-205 HK, Japan) and cyclic voltammetry (CV). An auto polarization system (HSV-100, Hakuto Denko, Japan) was used for the CV measurements. CV measurement was conducted using a 2 mm solution of the respective squaraine dyes and ferrocene (Fc) along with 0.1M tetrabutylammonium hexafluorophosphate as the supporting electrolyte in DMF. The HOMO energy level was calculated by measuring the shift in the oxidation potential of the dyes with respect to the oxidation potential of the Fc^+/Fc redox couple. Subsequently, LUMO energy level was estimated by adding the optical band gap (Eg) to the obtained HOMO value. Eg was calculated from energy corresponding to the optical absorption edge taken from the solid-state electronic absorption spectra of dyes adsorbed on the thin film of TiO_2.

2.2 Dye Adsorption behavior and its binding stability on TiO$_2$

Dye adsorption behavior was investigated using 4 μm thick transparent TiO$_2$ paste (1 cm^2 area) coated on the glass substrate. TiO$_2$ coated glass substrate were then dipped in 0.1 mM solution of the respective dyes and extent of dye adsorption as a function of time (until saturation) was monitored spectrophotometrically by measuring the absorbance of dyes at their absorption maximum (λ_{max}). Stability behavior of the dyes were investigated using glass substrate coated with mesoporous TiO$_2$ paste D/SP (Solaronix) having thickness of ~ 15 μm. TiO$_2$ coated glass substrates were dipped in 0.2 mM solution of the respective dyes in dehydrated ethanol until complete dye adsorption. Relative stability of these dyes on the TiO$_2$ was studied by putting the dye adsorbed TiO$_2$ substrate in the solvent mixture of acetonitrile and water (1:1) at room temperature and monitoring the extent of dyes desorbed from substrate to the solution. Quantitation of the desorbed dyes after 3 hours of dye desorption was carried out spectrophotometrically using standard calibration curves of the respective dyes. Remaining dyes on the mesoporous TiO$_2$ were then completely desorbed and quantitated using 40 mM NaOH solution in t-Butanol: Acetonitrile: Water: Ethanol solution taken in equal ratio.

2.3 Synthesis

Unsymmetrical squaraine dyes and their corresponding intermediates were synthesized as per the synthetic scheme shown in the Fig. 2. The intermediate 5-carboxy-1-ethyl-2,3,3-trimethyl-3H-indolium iodide (i) was synthesized and characterized as per our previous publication [27]. Starting compound 1,1,2-trimethylbenzo(e)indole [1] was purchased from Sigma-Aldrich and used without further purification.

2.3.1 Synthesis of 3-dodecyl-1,1,2-trimethyl-1H-benzo[e]indol-3-ium iodide [2]

6 g (28.7 mmol) of 1,1,2-trimethyl-2,3-dihydro-1H-benzo[e]indole [1] was taken in a round bottom flask with Propionitrile (40 mL) as the solvent. Then 12 g (43 mmol) of 1-Iodododecane (1.5 equivalent) was added to it. The mixture was then subjected to reflux at 110^0C for 26 hrs. Reaction monitoring was done by TLC in 15% ethyl acetate: Hexane solvent system. After the completion of reaction, the reaction mixture was cooled to room temperature followed by solvent evaporation. After complete evaporation of the solvent, ample diethyl ether was added to it followed by thorough ether washing. The residue was collected as a light pink solid to give the titled compound in 78 % yield (11.2 g). FAB-mass (measured m/z: 378.3164 [M] $^+$; calculated m/z: 378.3161).

2.3.2 Synthesis of (E)-4-((3-dodecyl-1,1-dimethyl-1H-3l4-benzo[e]indol-2-yl) methylene)-2-ethoxy-3-oxocyclobut-1-en-1-olate [3]

In a round bottom flask fitted with condenser, 1 equivalent of compound [2], (5 g, 9.9 mmol) and 1 equivalent of 3,4-Diethoxy-3-cyclobutene-1,2-dione 1.6 g (9.9 mmol) was taken in 25 mL ethanol. To it, 5 equivalent of trimethylamine (7.0 ml) was added. The reaction mass was then subjected to reflux for 6 hours, which soon turned to yellow color. The reaction mass was cooled, and the solvent was evaporated under vacuum. The obtained mass was then extracted with ethyl acetate followed by thorough washing with distilled water and brine. The obtained ethyl acetate layer was subjected to vacuum evaporation and finally the crude was purified by flash column chromatography with 10% Ethyl acetate: Hexane. The solvent was removed to get the tilted compound as yellow powder in 77 % yield (3.8 g). FAB-mass (measured m/z: 502.0 [M+H]$^+$; calculated m/z: 501.3).

2.3.3 Synthesis of (E)-4-((3-dodecyl-1,1-dimethyl-1H-benzo[e]indol-3-ium-2-yl)methylene)-2-hydroxy-3-oxocyclobut-1-en-1-olate [4]

3 g (6.0 mmol) of compound [3] was dissolved in 15 mL ethanol in a 50 mL round bottom flask. To this solution 5 equivalent 4N NaOH was added and refluxed for 2 hrs. The reaction mixture was cooled and the solvent was evaporated under vacuum. After complete evaporation of the solvent, the reaction mixture was acidified by diluted HCl and acidified crude was then extracted in chloroform and subjected to thorough washing by brine. The final hydrolyzed product was obtained as a red solid in 88 % yield (2.5 g).

2.3.4 Synthesis of 1-ethyl-5-hydroxy-2,3,3-trimethyl-3H-indol-1-ium iodide (ii)

The intermediate 5-hydroxy-2,3,3-trimethyl-3H-indole was synthesized following our previous work [28]. 1 equivalent 4 g (21.1 mmol) of 5-methoxy-2,3,3-trimethyl-3H-indole was dissolved in 20 mL dichloromethane. It was then cooled to 0^0C. To the cooled solution, 4 ml (2 eq.) of Boron tribromide was added dropwise followed by continuation of reaction at room temperature. The reaction progress was monitored by TLC and upon completion after 8 hours, the reaction was quenched by sodium thiosulphate followed by solvent extraction using ethyl acetate and thorough washing with distilled water followed by brine. The organic layer was evaporated under vacuum and the crude product was purified by column chromatography using 50% Ethyl acetate: Hexane. The desired product was obtained in 72 % yield (2.66 g). The obtained precursor 2.0 g (11.42 mmol) was dissolved in 10 ml acetonitrile. Then 2 equivalent (1.8 ml, 22.8 mmol) of 1-Iodoethane was added to it. The reaction mixture was then refluxed for 18 hours, while monitoring the progress by TLC. On completion, solvent was evaporated under vacuum and product was precipitated out adding diethyl ether. It was then filtered and the titled compound was obtained as pinkish solid in 63 % yield (2.3 g).

2.3.5 Synthesis of 5-sulfo-1-ethyl-2,3,3-trimethyl- -3H-indol-1-ium iodide (iii)

The intermediate was synthesized following the report by Park et al [29]. 5-Sulfo-2,3,3-trimethyl-3H-indole was synthesized by the reaction of 4-Hydrazino-benzenesulfonic acid hemihydrate 4 g (21.3 mmol) with 5 mL of 3-methyl-2-butanone in 20 mL acetonitrile under reflux for 7 hours. Reaction monitoring was done by TLC and upon completion of reaction, solvent was evaporated and the crude was purified by column chromatography to give the product in 75 % yield. 2.5 g (10.4 mmol) of this compound was dissolved in 15 ml of acetonitrile and 2 equivalents of 1-Iodoethane (4 ml, 20.8 mmol) was added. The mixture was then refluxed for 12 hours while monitoring the reaction progress by TLC. The solvent was evaporated under vacuum and ample diethyl ether was added for precipitation, which was filtered to get the titled compound as pinkish solid in 68 % yield (2.8 g).

2.3.6 Synthesis of 5-(diethoxyphosphoryl)-1-ethyl-2,3,3-trimethyl-3H-indol-1-ium iodide (iv)

The compound was synthesized by slightly modified procedure as reported Archer et al [30]. To a solution of 4-Iodoindole (1g, 3.5 mmol) in toluene was added Tetrakis (triphenylphosphine) palladium (0) (0.18 mmol), and triethylamine (12.4 mmol) followed by addition of Diethylphosphite (0.31 mmol) and reaction mixture was refluxed for 12 hrs. Upon completion of reaction as monitored by TLC, solvent was evaporated. Product was extracted with ethyl acetate and washed with water and brine. Finally, it was purified by column chromatography giving desired compound diethyl (2,3,3-trimethyl-3H-indol-5-yl) phosphonate as colorless liquid. To a solution of this compound in acetonitrile was added ethyl iodide flowed by reflux for 12 hrs. Upon completion of reaction, solvent was evaporated followed by precipitation using diethyl ether. It was then filtered, washed with diethyl ether and dried under vacuum to obtain the titled compound 5-(diethoxyphosphoryl)-1-ethyl-2,3,3-trimethyl-3H-indol-1-ium iodide (iv).

2.3.7 Synthesis of SQ-138

To a 50 mL round bottom flask, 1 equivalent of 5-carboxy-1-ethyl-2,3,3-trimethyl-3H-indol-1-ium iodide (i), (300 mg, 1.3 mmol), 1 equivalent (559 mg, 1.3 mmol) of hydrolyzed semi squaraine dye intermediate [4] and 30 mL of 1:1 toluene/n-butanol were added. The reaction mixture was refluxed for 12 hours, which soon turned greenish. Reaction monitoring was done by TLC, solvent was evaporated under vacuum after completion and the crude was purified by column chromatography using 5% methanol: chloroform solvent. The evaporation of the collected compound fraction afforded the desired 450 mg of the compound as a vibrant blue color in 51 % yield. Results of HR-FAB-MS (measured m/z: 686.4114 [M]$^+$; calculated m/z: 686.4084) and ^{1}H NMR (500 MHz, CDCl$_3$): δ/ppm= 8.15(dd,H-44); 8.05(dd,H-41); 7.9(dd,H-8); 7.86 (dd,H-9); 7.55(dd,H-45); 7.41(t,H-6); 7.39(t,H-5); 7.27(d, H-7); 6.9(d,H-4); 6.08(s,H-33); 5.9(s,H-28); 4.14 (m,H-46); 3,98(t,H-16); 2.10(t,H-47); 1.82(m,H-17); 1.77(s,H39+40); 1.56(s, H14+15); 1.40(m,H-18), 1.39 (m,H-19); 1.38 (m,H-20),1.37(m,H-21), 1.34(m,H-22);1.33 (m,H-23); 1.31 (m,H-24);1.29 (m,H-25); 1.28(m, H-26), 1.22(t,H-27) confirms the structural identity of this dye.

2.3.8 Synthesis of SQ-141

1 equivalent of 1-ethyl-5-hydroxy-2,3,3-trimethyl-3H-indol-1-ium iodide (ii) 300 mg (0.91 mmol) of and 1 equivalent (392 mg) of semi squaraine dye intermediate [4] was dissolved in 30 mL of 1:1 toluene/n-butanol in a round bottom flask fitted with condenser. The reaction mixture was refluxed for 18 hours. After complete removal of the solvent, the crude was subjected to flash column chromatography with chloroform methanol as the eluting agent to afford a vibrant blue solid (285 mg) in 43% yield. HR-FAB-MS (measured m/z: 658.4131 [M]$^+$; calculated m/z: 658.4134). ^{1}H NMR (500 MHz, CDCl$_3$): δ/ppm= 9.74.15(dd,H-43); 8.12(dd,H-41); 7.82(dd,H-8);

7.79 (dd,H-9); 7.51(dd,H-44); 7.49(t,H-6); 7.48(t,H-5); 7.20(d, H-7); 6.8(d,H-4); 5.9(s,H-33); 5.89(s,H-28); 4.02(m,H-45); 3.58(t,H-16); 2.10(t,H-46); 1.98(m,H-17); 1.78(s,H39+40); 1.50(s, H14+15); 1.41(m,H-18), 1.40(m,H-19); 1.38(m,H-20); 1.37(m,H-21), 1.34(m,H-22); 1.32(m,H-23); 1.31(m,H-24); 1.29(m,H-25); 1.28(m, H-26), 1.21(t,H-287).

2.3.9 Synthesis of SQ-142

To a round bottom flask fitted with condenser, 400 mg (1.5 mmol) of 5-sulfo-1-ethyl-2,3,3-trimethyl-3H-indol-1-ium iodide and 1 equivalent (646 mg) of semi squaraine dye intermediate [4] was dissolved in 30 mL of 1:1 toluene/n-butanol. The reaction mixture was then refluxed for 18 hours. Thereafter the solvent was evaporated and the crude was purified with column chromatography using chloroform methanol solvent system. 400 mg of the desired compound was collected as a blue solid in 40 % yield. HR-FAB-MS (measured m/z: 722.3759 [M]$^+$; calculated m/z: 722.3753). ^{1}H NMR (500 MHz, CDCl$_3$): δ/ppm= 9.73(dd,H-44); 8.12(dd,H-41); 7.81(dd,H-8); 7.79(dd,H-9); 7.50(dd,H-45); 7.39(t,H-6); 7.35(t,H-5); 7.19(d,H-7); 6.9(d,H-4); 4.04(s,H-33); 4.02(s,H-28); 3.67(m,H-46); 3.63(t,H-16); 2.14(t,H-47); 2.06(m,H-17); 1.84(s,H39+40); 1.56(s, H14+15); 1.44(m,H-18), 1.42(m,H-19); 1.39(m,H-20); 1.36(m,H-21), 1.34(m,H-22); 1.33(m,H-23); 1.31(m,H-24); 1.29(m,H-25); 1.28(m,H-26), 1.27(t,H-27).

2.3.10 Synthesis of SQ-143

315 mg of 5-(diethoxyphosphoryl)-1-ethyl-2,3,3-trimethyl-3H-indol-1-ium iodide (iv) and 302 mg of semi squaraine dye intermediate [4] was dissolved in 1:1 toluene/n-butanol in a round bottom flask. The reaction mixture was then refluxed for 18 hours. The solvent was evaporated and the crude was subjected to flash column chromatography using chloroform methanol as the eluting

system. After the evaporation of the collected pure fraction, 220 mg of compound was obtained as a blue solid in 54.3 % yield. On hydrolysis of Ester by using TMS-Br in DCM at room temperature for 6-8 hrs. Reaction monitoring has been done by TLC using Methanol chloroform as mobile phase. Purified the product by column chromatography by using Methanol chloroform as solvent. After the evaporation of the collected pure fraction, 130 mg of the titled compound was obtained as a blue solid in 63.7 % yield. HR-FAB-MS (measured m/z: 723.3938 $[M+H]^+$; calculated m/z: 722.3849). ^{1}H NMR (500 MHz, CDCl$_3$): δ/ppm= 9.73(dd,H-44); 8.07(dd,H-41); 7.85(dd,H-8); 7.82(dd,H-9); 7.53(dd,H-45); 7.40(t,H-6); 7.37(t,H-5); 7.29(d,H-7); 6.97(d,H-4); 6.43(s,H-33); 6.14(s,H-28); 4.24(m,H-46); 3.9(t,H-16); 3.79(t,H-47); 3.45(m,H-17); 1.57(s,H39+40); 1.38(s, H14+15); 1.26(m,H-18), 1.20(m,H-19); 1.18(m,H-20); 1.17(m,H-21), 1.15(m,H-22); 1.13(m,H-23); 1.14(m,H-24); 1.04(m,H-25); 1.03(m,H-26), 0.82(t,H-27).

2.4 DSSC fabrication and characterization

Fluorine doped Tin oxide (FTO) coated glass substrate was used to prepare the photoanode of the DSSC. FTO was coated with TiO$_2$ paste D/SP by screen-printing followed by sintering at 450 ^{0}C and this process was repeated in order to attain the thickness of the mesoporous TiO$_2$ to be about 12 μm. The substrate was then dipped in to the solution of 0.2 mM of the respective dyes and 20 mM of the dye aggregation preventing agent chenodeoxycholic acid (CDCA) in dehydrated ethanol for 4 hours. A catalytic Pt sputtered FTO glass was employed as counter electrode. Iodine based redox electrolyte (I$_3^-$/I$^-$) containing LiI (0.5 M), iodine (0.05 M), t-butyl pyridine (0.5 M), 1,2-dimethyl-3-propylimidazolium iodide (0.6 M) in acetonitrile was used for DSSC fabrication and Sandwiched between the working electrode and counter electrode. Device was finally sealed using 20 μm hot melt spacer and epoxy resin. Performance of the solar cells were evaluated using

solar simulator (CEP-2000 Bunko Keiki Co. Ltd, Japan) equipped with a xenon lamp (Bunko Keiki BSO-X150LC) used as a source of simulated solar irradiation at 100 mW/cm^2, AM 1.5 G.)

3. Results and Discussion

3.1 Optical Characterizations

3.1.1 Electronic absorption spectra

Electronic absorption spectra of the unsymmetrical squaraine dyes were recorded in 5µM ethanol solution and shown in the Fig. 3. It can be clearly seen from this figure that the dyes exhibit very sharp, intense and narrow light absorption mainly in the far-red (550 nm -700 nm) wavelength region of the solar spectrum. At the same time, they exhibit very high molar extinction coefficients (ε) in the range 1-3 x 10^5 dm^3.mol^{-1}.cm^{-1}. The ε values shown by the dyes are about 10 times higher than that of the typical ruthenium complex based sensitizer like N3 [31]. Appreciably high molar extinction coefficient could be due to the intramolecular charge transfer characteristics along with the extended π-electron donor network, π-π* electronic transition and also due to the presence of central squaric acid moiety having a strong electron withdrawing nature [32]. It can also be seen from this figure that dyes SQ-142 and SQ-143 bearing sulfonic acid and phosphonic acid functional groups, respectively, exhibit relatively red-shifted absorption maximum (λ$_{max}$) at 668 nm, which could be attributed to the extended π-conjugation contributed from the S and P atoms of the anchoring groups. The relatively higher ε values of these sensitizers are also beneficial for transparent/semitransparent DSSCs, since even with thin layers of mesoporous TiO$_2$ sufficient photons can be easily absorbed.

3.1.2 Florescence emission spectra

Fluorescence emission spectra of these dyes were also recorded in the ethanol solution and shown in the Fig. 3 along with the summarization of optical parameters in the table 1. It can also be seen from this figure that emission spectra of the dyes reveal similar mirror image like spectral pattern with narrow spectral width and emission maxima shifted to the longer wavelength region with the offset above 700 nm. Wavelength difference between absorption maximum and emission maximum (Stokes shift) was also calculated and shown in the table 1. A perusal of the Fig. 3 and table 1 reveals that this shift was relatively small for dyes under investigation as compared to typical visible sensitizers used in the DSSC research. The small Stokes shift of 12-17 nm only is benign for the DSSCs purpose as the smaller shift depicts the conformational rigidity of the molecules in the excited state [33]. SQ-142 with sulphonic acid anchoring group possess the minimal stokes shift of only 12 nm signifying the highest conformational stability.

3.2 Electrochemical Characterization

Squaraine dyes typically exhibit good electrochemical activity with pronounced redox behavior typically showing two oxidation peaks and one reduction peak. It has been demonstrated that these dyes exhibit extremely high electrochemical stability, where, there was practically no change in the shape and position of the redox peaks even after 3500 continuous redox cycles [34]. Cyclic voltammetry (CV) has been widely used in DSSC research not only for electrochemical characterization but also as a convenient tool for the estimation of the energy of HOMO corresponding to first oxidation peak of the sensitizers. In this work, CV of unsymmetrical squaraine dyes was recorded in DMF solution along with ferrocene using similar electrode, electrolyte and scan rate, which is shown in the Fig. 4. A perusal of CV of squaraine dyes having

different functional group reveals that introduction of electron withdrawing groups like -COOH (SQ-138), –SO$_3$H (SQ-143) and -PO$_3$H$_2$ (SQ-143) shifts the oxidation peak towards higher potential as compared to that of electron donating –OH group (SQ-141) containing squaraine dye. This could be attributed to the stabilization of molecular orbitals upon introduction of functional groups with electron withdrawing nature. In this work, potential corresponding to 1st oxidation wave of the dyes has been used to estimate the HOMO energy level of dyes. Shift in oxidation potential of the dyes with respect to the oxidation potential Fc/Fc$^+$ redox couple was used to calibrate the HOMO energy level of dyes with respect to the vacuum level. The HOMO value of the dyes was calculated from the shift in the oxidation peak with respect to the Fc/Fc$^+$, whose value was taken as -5.01 eV as per the report by Su and Girault [35]. HOMO energy level of the dyes thus calculated was used to construct the energy band diagram of dyes.

3.3 Energy Band Diagram

Energetic matching amongst the components of DSSC like mesoporous oxide semiconductor, sensitizing dye and redox electrolyte is crucial for the functioning of DSSCs. On excitation by photon flux, electron from the HOMO of the dye gets excited to its LUMO, which is then injected to the conduction band (CB) of the TiO$_2$ and the excited dye molecules are regenerated by the electron from the redox electrolyte. This suggests that there should be energetic cascade between the two states of dye with respect to the TiO$_2$ and redox electrolyte to maintain the feasible electron flow. Thus the energetic matching of sensitizers with respect to the wide band gap semiconductor and redox electrolyte is one of the most important requirements for the suitability as sensitizer of the DSSCs. Therefore, energy band diagram of sensitizing dyes for DSSC application was constructed considering TiO$_2$ and I$^-$/I$_3^-$ as the most commonly utilized wide band gap

semiconductor and redox electrolyte, respectively. To accomplish this, CB energy level of TiO_2 and redox energy level of the electrolyte was taken to be -4.00 eV and -4.90 eV, respectively, as per the previous reports [36].

As mentioned earlier, HOMO energy level of the dyes was estimated from the CV, while energy of the LUMO was estimated by the relation, LUMO = HOMO + Eg, where Eg is optical band gap estimated from the optical absorption edge of electronic absorption spectra of dyes adsorbed on thin transparent films of TiO_2. A perusal of the energy band diagram shown in the Fig. 5 clearly corroborates that LUMO energy level of all of the sensitizers are higher than that of the CB energy level of TiO_2 ensuring the facile electron injection after the photoexcitation. At the same time, lower HOMO energy level of the dyes with respect to I^-/I_3^- redox energy level ensures that oxidized dyes after the electron injection can be regenerated too. In this regards, we can see that the dye SQ-142 bears the lowest HOMO, which could be attributed to the relatively strong electron withdrawing nature of $-SO_3H$ anchoring group leading to stabilization of molecular orbitals and is in accordance with CV results. On the other hand, SQ-141 with $-OH$ anchoring group seems to be a non-optimal sensitizer owing to its shallow HOMO energy level leading to difficulty in the regeneration of oxidized dye. Relatively upward shift of HOMO energy of this dye could be attributed to the presence of electron donating nature of the hydroxyl group.

3.4 Theoretical Molecular Orbital Calculation

In the recent past, a lot of research on the MO calculations have been extensively performed in the DSSC research aiming towards design and development of novel sensitizers by prior prediction of their energetics and electronic absorption spectra. Amongst them, TD-DFT has been widely used

due to its reliable prediction of energetics and electronic absorption spectra of the functional molecules [37]. The geometries of squaraine dyes under investigation were optimized using (6-311G) basis set and B3PW91 hybrid functional as implemented in the Gaussian 09 based on its reliability as per our earlier publications [27,38]. Along with the structural optimization of the squaraine dyes, energy of the HOMO and LUMO for respective dyes was theoretically calculated and shown in the parentheses of the Fig 6. Upon comparison of the theoretical value of HOMO of the dyes with their respective experimental data, it can be clearly seen that there is very good match between the experimental and theoretically predicted results. Thus, an estimation closer to the real value could be imbibed with this functional and basis set, which could make the design of novel sensitizers easier. The optimized geometry along with distribution of electron density in the HOMO and LUMO of the unsymmetrical squaraine dye bearing –COOH functional group (SQ-138) is shown in the Fig. 6.

It can be seen that electron density distributions in the HOMO of this dye is mainly concentrated at the central squaric acid core and slightly extended to the π-framework attached near to the core of the dye molecule. However, in the LUMO, it exhibits relatively reduction near the squaric acid core and dominance of electron density towards anchoring group bearing indole unit indicating the possibility of intramolecular charge transfer (ICT) and indicates the feasibility of charge separation on excitation. Presence of sufficient electron density at the anchoring group of a sensitizer ensures good electronic coupling between the excited dye molecule and vacant d-orbitals of the wide-band gap semiconductor (TiO_2 in present case). This ensures the facile electron injection if LUMO energy level of the dye lies is above the CB energy level of electron accepting TiO_2. It can be seen from the Fig. 6 that electron density distribution in the LUMO of

unsymmetrical squaraine dyes SQ-138 and SQ-142 bearing –COOH and -SO$_3$H anchoring groups not only lies in the same plane of the main molecular framework and exhibit ICT but also diversion of sufficient electron density at the anchoring group. This suggest their suitability as sensitizer of DSSC, since both of them possess a sufficient driving force for electron injection in the CB of TiO$_2$. On the other hand, the other two dyes SQ-141 and SQ-143 bearing –OH and –PO$_3$H$_2$ anchoring groups not only lacks prominent ICT but also appears to face hindrance in the electron injection in due to the low electron density on LUMO in spite of sufficient driving force for the electron injection. This also explains the reason behind relatively lower photovoltaic performance of dyes bearing -PO$_3$H$_2$ anchoring groups as compared to that of their –COOH anchoring group counterparts [39-40]. As discussed earlier, energetics of the photo functional molecules plays a dominant role for their utilization as sensitizers in the DSSCs, therefore, their prior accurate prediction is expected to accelerate the development of novel sensitizers.

3.5 Dye adsorption behavior on mesoporous TiO$_2$

Sensitizing dyes are adsorbed onto the surface of wide band gap semiconductors via suitable chemical linkage (ester linkage by –COOH containing dyes) and nature of this not only controls the electron injection but also imparts stability to the DSSCs. Therefore, the optimal fixation of the dyes with the help of anchoring group onto the semiconductor surface is crucial for the proper functioning of the DSSCs [41]. At the same time, optimal adsorption of sensitizing dyes on the mesoporous TiO$_2$ is also the important step for the fabrication of photo anode of DSSCs. A complete coverage by monolayer of sensitizing dyes on the TiO$_2$ nanoparticle is more desirable for the optimal performance of the photoanode. The incomplete dye coverage results in drawbacks like insufficient photon harvesting as well as back electron transfer from electrons injected in TiO$_2$

and oxidized dye or electrolyte [42]. On the other hand, excess amount of the dye loading onto the TiO$_2$ leads to unwanted dye aggregation resulting in to poor electron injection [43]. Adsorption behavior and binding strength of the dye onto the mesoporous TiO$_2$ along with their diffusion rate through the Nano pores in the mesoporous TiO$_2$ depends on the structure of the dye molecules, nature of the anchoring group and their interaction of with the TiO$_2$ [44]. Investigation in this context on visible sensitizers are although available but for NIR dyes with varying anchoring group is still lacking [45-46]. Figure 8 depicts the adsorption behavior of the unsymmetrical squaraine dyes bearing different anchoring groups on the thin films of the mesoporous TiO$_2$.

A perusal of the Fig. 7(a) reveals that upon adsorption of dyes on to the mesoporous TiO$_2$, not only there is slight red-shift in the λ_{max} of the respective dyes as compared to that of in solution (Fig. 3) but also spectral broadening and pronounced appearance of vibronic shoulders. This is attributed to the enhanced intermolecular interactions in the condensed state and enhancement in the vibronic shoulders indicates the aggregate formation. Relative ratio of the absorbance of vibronic shoulder to the main peak associated with the monomeric dye has been reported to be index of molecular aggregation [47-48]. It can be clearly seen that extent of aggregation for SQ-138 bearing carboxylic anchoring group is higher as compared to that of SQ-143 bearing phosphonic acid anchoring group. This can be explained considering the fact that contrary to the –COOH group lies in the same plane of the dye framework, non-planarity of phosphonic acid group hinders the aggregation. At the same, time SQ-142 bearing sulfonic acid anchoring group not only exhibit clear vibronic peak but also additional absorption peak in the 450 nm-550 nm, which is not present in the other dyes. This could be attributed to the extensive aggregate formation, which is not only due to planarity of sulfonic acid but also promotion of hydrogen bonding amongst dye molecules during adsorption due to presence of two S=O bonds. Kim et al. [49] have also

observed aggregation induced blue shifted light absorption in squaraine dyes and emphasized that some squaraine surfactants easily form blue shifted H-aggregates on SnO_2 surfaces absorbing around 500 nm wavelength region. In fact, we have also previously demonstrated that absence of alkyl substitution in symmetrical squaraine dyes leads to pronounced blue shifted H-aggregates, which diminishes upon alkyl substitution [50].

A swift adsorption of dye molecules on mesoporous wide band gap semiconductor in combination with strong binding is highly desired for the industrialization of DSSCs. Implication of nature of anchoring groups on their adsorption behavior on the thin films of mesoporous TiO_2 was conducted by monitoring the extent of adsorbed dyes as function of time spectrophotometrically. Rate of dye adsorption was estimated by monitoring change the peak absorbance of the respective dyes after different time intervals of the dye adsorption, which has been shown in the Fig. 7(b). A perusal of the this figure clearly corroborates that squaraine dyes bearing carboxylic (SQ-138) and phosphonic acid (SQ-143) adsorb more swiftly as compared to that bearing sulfonic acid (SQ-142) and hydroxyl groups (SQ-141) and rate of dye adsorption follows the order $-COOH>-PO_3H_2>>-OH>-SO_3H$. Adsorption of sensitizing dyes starts with activation of the OH groups on the TiO_2 surface by functional group present on the dye via protonation followed by chemical bonding. Therefore, activation should be controlled by the pKa values of the functional groups, which follows the order $-COOH>-PO_3H_2>-OH$ [51]. It was highly surprising that sensitizing dye SQ-142 exhibited slowest rate of dye adsorption on the TiO_2 in spite of extremely high pKa $-SO_3H$ functional group. At present actual reason for such a drastically low rate of dye adsorption is not known but presumably, it might be associated with the very high aggregation tendency of this dye molecule as depicted by the solid state electronic absorption

spectra shown in the Fig. 8(a). During the dye adsorption process, it seems that formation of large aggregates hampers the adsorption of other incoming new dye molecules on the non-adsorbed TiO_2 surface.

3.6 Anchoring stability dyes on mesoporous TiO_2

In order to evaluate the anchoring stability of unsymmetrical squaraine dyes on the mesoporous TiO_2, dye desorption experiment was conducted. To estimate, total dye loading, after complete dye adsorption, it was completely desorbed from the surface using a solvent mixture of acetonitrile, tert. Butanol, water and NaOH. For relative dye stability studies, dye adsorbed TiO_2 substrate of respective dye, was put in 1:1 (V/V) mixture of acetonitrile and water at room temperature and amount of dye desorbed after 3 hours in each case was estimated spectrophotometrically. Results of dye desorption for the photoanodes fabricated using dyes bearing different anchoring groups are summarized in the table-2.

A perusal of the table 2 clearly corroborates that under identical conditions of dye desorption on TiO_2 such as thickness, area and time of desorption, sensitizing dyes exhibit differential binding strength on the mesoporous TiO_2 as estimated by the percentage removal dyes upon putting them in to acetonitrile- water mixture after 3hrs. It is worth to mention here that weakest binding was exhibited by SQ-142 bearing sulfonic acid anchoring group (99.3 % removal), while SQ-143 bearing phosphonic acid anchoring group, exhibited strongest binding (1.1 % removal). This suggested that SQ-143, which is containing PO_3H_2 functional group exhibited highest stability on the mesoporous TiO_2 as compared to dyes bearing other functional groups. SQ-143 exhibited highest dye loading (228.70 nmol/cm^2), which was significantly higher than that of SQ-138 (30.48 nmol/cm^2), bearing most commonly utilized –COOH functional group, which

might be attributed to the presence of two-OH functionality of the phosphonic acid anchoring group. Based on dye desorption studies conducted under identical experimental conditions, relative binding strength on the mesoporous TiO_2 follows the order $–SO_3H<-COOH<-OH<<-PO_3H_2$.

3.7 Photovoltaic characterization

In order to investigate the nature of anchoring groups on the photovoltaic behavior, DSSCs were fabricated using unsymmetrical squaraine dyes as sensitizer, mesoporous TiO_2 as dye adsorption/ electron transporting scaffold and most commonly used iodine based (I^-/I_3^-) redox electrolyte followed by photovoltaic characterization after simulated solar irradiation of 100 mW/cm². In each case, 20 mM of CDCA was used as co-adsorber in order to prevent the dye aggregation along with 0.2 mM of respective dyes during the dye adsorption. Figure 9 depicts the photovoltaic characteristics of the DSSCs using different squaraine dyes along with the summarization of the photovoltaic parameters in terms of short-circuit current density (Jsc), open circuit voltage (Voc), fill factor (%) and efficiency in the table-3. It can be seen from the Fig. 8 and table 3 that DSSC fabricated with SQ-138 bearing carboxylic acid anchoring group exhibited the best photovoltaic performance with photoconversion efficiency (PCE) of 4.07 %, while the poorest performance (PCE = 0.63) was observed in the case of DSSC based on SQ-141 bearing –OH anchoring group. One of the possible causes for the poorest performance exhibited by SQ-141 could be attributed to the energetic mismatch of this dye with respect to redox energy level of iodine-based electrolyte as shown in the Fig. 5.

A very small driving force for the dye regeneration leads to pronounced back electron transfer after the photoexcitation leading to hampering in both of the Jsc as well as Voc. It is interesting to note that SQ-143 with phosphonic acid anchoring group exhibited much hampered

photovoltaic performance with PCE of 1.03 % as compared to that of DSSC based on SQ-138 bearing –COOH. Even though SQ-143 possesses a number of favorable conditions required for a sensitizer like high dye loading, binding strength (table 2) and suitable energetic cascade for electron injection and dye regeneration (Fig. 5). This could be attributed to tetrahedral nature of phosphonic acid as compared to that of planer carboxylic acid leading to relatively small diversion of electron density at LUMO as shown in the Fig. 6. This represents small ICT and hampered electronic coupling with the 3d orbitals of TiO_2 leading to hampered electron injection ultimately resulting in to very poor photovoltaic performance.

Looking for the results shown in the table 2 for the dye adsorption behavior table 3 for photovoltaic parameters, one can argue that there was a differential dye adsorption depending on the nature of the anchoring group and amount of the dyes present on the photoanode have also good impact on controlling the overall PCE. In order to clarify this issue, DSSCs were also fabricated for fixing of the amount of adsorbed dyes to be about 20 nmol/cm^2. This was achieved by decreasing the dye adsorption time for SQ-138 and SQ-143, while increasing for the SQ-141. Photovoltaic characteristics for the DSSCs fabricated under this condition is shown in the Fig. 9 along with the summarization of the photovoltaic data in the table 4. A perusal of the data shown in the Fig. 9 and table 4 clearly corroborates that overall PCE for the DSSCs using SQ-138 and SQ-143 was decreased, while there was an increase for the SQ-141 as compared to that shown in the table 3. Main controlling parameter for this change was basically Jsc. This is attributed to that fact that dye loading for SQ-138 and SQ-143 was relatively small under this condition and there is a need of optimal dye amount for obtaining the best PCE for that system. On the other hand, increase in the dye loading for SQ-141 might be responsible for slight increase in the PCE under

present condition. Therefore, presence of an optimal dye loading for a given system is highly desired to extract the best performance apart from other controlling parameters like energetic matching and good electronic coupling with TiO$_2$ as discussed previously.

Apart from controlling the electron injection, anchoring group of the sensitizer plays a vital role in controlling the overall stability of the DSSCs. In the section, 3.6 we have demonstrated that excluding the dye SQ-141 due to lack of energetic matching and small ICT, anchoring stability of mesoporous TiO$_2$ follows the trend –SO$_3$H<-COOH<<-PO$_3$H$_2$ based on dye desorption data shown in the table 2. In order to strengthen this observation, investigation pertaining to the stability of the DSSCs fabricated using these dyes were also conducted under continuous 1 Sun (100 mW/cm2) light irradiation for different time intervals followed by the photovoltaic measurements. Variation in the normalized PCE for the DSSCs bearing unsymmetrical squaraine dyes with different anchoring group is shown in the Fig. 10. It can be clearly seen from this figure that SQ-143 bearing -PO$_3$H$_2$ anchoring group shows extremely high device stability, where practically there was no change in the PCE even after 3 hours of continuous 1 Sun light irradiation. Contrary to this, there was about 8 % and 35 % fall in the PCE for DSSCs based on dyes SQ-138 and SQ-142 bearing -COOH and –SO$_3$H anchoring groups, respectively.

One can argue that stability data shown in the Fig. 10 are taken for very short period of time of only 3 hours and there was a drastic decrease in the PCE of SQ-138 bearing –COOH, while there are many reports of sensitizers bearing –COOH group with fairly good stability. This is attributed to the fast removal of the volatile acetonitrile solvent due to heating of the DSSCs under continuous 1 Sun solar irradiation. This the reason why, either electrolyte using high boiling

solvents like propionirile, ionic liquids or quasi-solid gel electrolytes have quite frequently used for the long term stability studies. To clarify this, DSSCs using sensitizers with varying anchoring groups were fabricated and stored at room temperature and photovoltaic performance after simulated 1 Sun solar irradiation was measured after different time intervals (contrary to continuous light irradiation) and monitored for a period of two weeks. Normalized PCE for DSSCs have been shown in the Fig. 11. It can be seen from the Fig. 11 that DSSCs fabricated using squaraine dyes with different anchoring exhibited retention of about 80 % of initial PCE even after the two weeks. A careful perusal reveals that even storing of the DSSCs at the room temperature, there was a slow removal of acetonitrile solvent leading the decrease in the PCE, which was re-gained after further injection of electrolyte as indicated by the arrows. Nevertheless, this regain was differential depending on the nature of anchoring groups of the sensitizers. This regain was 100 % for the DSSC based on dye SQ-143 bearing phsophonic acid anchoring group. On the other hand, slope of the average fall in the PCE follows the same order of $-SO_3H < -COOH << -PO_3H_2$. Thus the observed trend of DSSC stability was same as that of the anchoring stability of dyes on the mesoporous TiO_2. Therefore, trend of anchoring stability of the dyes on the mesoporous TiO_2 get directly translated in to overall device stability.

Conclusion

In summary, we have designed and synthesized four novel unsymmetrical squaraine dyes having same main molecular framework but different anchoring groups such as carboxylic acid, hydroxyl, sulfonic acid and phosphonic acid along with excellent solubility in the majority of organic solvent. After successful synthesis and characterization, they have been subjected to photophysical investigation utilizing, electronic absorption spectroscopy, fluorescence emission spectroscopy,

cyclic voltammetry, construction of energy band diagram and theoretical MO calculation using Gaussian G09. Investigation of adsorption behavior of these dyes on mesoporous TiO_2 revealed the rate of dye adsorption following the order SQ-138>SQ-143>SQ-141>SQ-142, while desorption studies indicated that binding strength on the mesoporous TiO_2 follows the order SQ-143>>SQ-141>SQ-138>SQ-142. Squaraine dye with phosphonic acid anchoring group exhibited about 70 times higher binding strength as compared to that of most commonly employed –COOH anchoring group containing squaraine dye. Theoretically predicted value of HOMO energy for all of the sensitizers are in very well agreements with the corresponding experimental values obtained by cyclic voltammetry. Theoretical MO calculation pertaining to the electron density distribution in HOMO and LUMO indicated good ICT and possibility of strong electronic coupling with TiO_2 for the dyes bearing –COOH (SQ-138) and –SO_3H (SQ-142) functional groups, which is also supported by the their relatively improved photovoltaic performance as compared to other anchoring groups. Energy band diagram has clearly indicated that except SQ-141 bearing hydroxyl anchoring group form energetic cascade with respect to CB of TiO_2 and redox energy level of I_3^-/I^-, which is responsible for its poorest photovoltaic performance. In spite of very good dye loading, very high binding strength and favorable energetic cascade, SQ-143 exhibited highly hampered photovoltaic performance as compared to that of SQ-138, which was attributed to poor ICT and electronic coupling with TiO_2 as indicated by theoretical MO calculations. DSSC stability data using dyes with different anchoring group clearly corroborates the same trend as to that observed for the anchoring stability of the dyes on the mesoporous TiO_2.

References

1. Z. Bao, Materials and Fabrication Needs for Low-Cost Organic Transistor Circuits, Adv. Mater. 12 (2000) 227-230.

2. H. E. Katz, Z. Bao, S. L. Gilat, Synthetic Chemistry for Ultrapure, Processable, and High-Mobility Organic Transistor Semiconductors, Acc. Chem. Res. 34 (2001) 359–369.

3. J.-M. Zhou, W. Shi, N. Xu, P. Cheng, Highly Selective Luminescent Sensing of Fluoride and Organic Small-Molecule Pollutants Based on Novel Lanthanide Metal–Organic Frameworks, Inorg. Chem. 52 (2013) 8082–8090.

4. C. Wang, T. Zhang, W. Lin, Rational Synthesis of Noncentrosymmetric Metal–Organic Frameworks for Second-Order Nonlinear Optics, Chem. Rev. 112 (2012) 1084–1104.

5. B. O'regan, M. Grätzel, A low-cost, high-efficiency solar cell based on dye-sensitized colloidal TiO_2 films, Nature 353 (1991) 737–740.

6. L. S.-Mende, U. Bach, R. H.-Baker, T. Horiuchi, H. Miura, S. Ito, S. Uchida, M. Grätzel, Organic Dye for Highly Efficient Solid-State Dye-Sensitized Solar Cells, Adv. Mater. 17 (2005) 813 - 815.

7. A. Mishra, M. K. R. Fischer, P. Bäuerl, Metal Free Organic Dyes for Dye-Sensitized Solar Cells: From Structure: Property Relationships to Design Rules, Angew. Chem. Int. Ed. 48 (2009) 2474 – 2499.

8. C. Anselmi, E. Mosconi, M. Pastore, E. Ronca, F. De Angelis, Adsorption of organic dyes on TiO_2 surfaces in dye-sensitized solar cells: interplay of theory and experiment, Phys. Chem. Chem. Phys. 14 (2012) 15963–15974.

9. R. Grisorio, L. D. Marco, C. Baldisserri, F. Martina, M. Serantoni, G. Gigli, G. P. Suranna, Sustainability of Organic Dye-Sensitized Solar Cells: The Role of Chemical Synthesis, ACS Sustainable Chem. Eng. 3 (2015) 770−777.

10. S. Ko, H. Choi, M.-S. Kang, H. Hwang, H. Ji, J. Kim, J. Ko, Y. Kang, Silole-spaced triarylamine derivatives as highly efficient organic sensitizers in dye-sensitized solar cells (DSSCs), J. Mater. Chem. 20 (2010) 2391-2399.

11. Z. Ning, Q. Zhang W. Wu, H. Pei, B. Liu, H. Tian, Starburst Triarylamine Based Dyes for Efficient Dye-Sensitized Solar Cells, J. Org. Chem. 73 (2008) 3791-3797.

12. N. Koumura, Z.S. Wang, M. Miyashita, Y. Uemura, H. Sekiguchi, Y. Cui, A. Mori, S. Mori, K. Hara, Substituted carbazole dyes for efficient molecular photovoltaics: long electron lifetime and high open circuit voltage performance, J. Mater. Chem 19 (2009) 4829-4836.

13. K. Hara, Z.S. Wang, Y. Cui, A. Furube, N. Koumura, Long-term stability of organic–dye-sensitized solar cells based on an alkyl-functionalized carbazole dye Energy Environ. Sci. 2 (2009) 1109-1114.

14. A. Burke, L. S.M., S. Itoa, M. Grätzel, A novel blue dye for near-IR 'dye-sensitised' solar cell applications, Chem. Commun. 3 (2007) 234-236.

15. L. Zhang, X. Yang, W. Wang, G. G. Gurzadyan, J. Li, X. Li, J. An, Z. Yu, H. Wang, B. Cai, A. Hagfeldt, L. Sun, 13.6% Efficient Organic Dye-Sensitized Solar Cells by Minimizing Energy Losses of the Excited State, ACS Energy Letters.4 (2019) 943.

16. A. Pradhan, M. S. Kiran, G. Kapil, S. Hayase, S.S. Pandey, Synthesis and Photophysical Characterization of Unsymmetrical Squaraine Dyes for Dye-Sensitized Solar Cells Utilizing Cobalt Electrolytes, ACS Appl. Energy Mater. 1 (2018) 4545–4553.

17. L. Hu, Z. Yan, H. Xu, Advances in synthesis and application of near-infrared absorbing squaraine dyes, RSC Advances 3 (2013) 7667-7676.

18. D. G. Brown, P. A. Schauer, J. B.-Garcia, B. R. Fancy, C. P. Berlinguette, Stabilization of Ruthenium Sensitizers to TiO_2 Surfaces through Cooperative Anchoring Groups, J. Am. Chem. Soc. 135 (2013) 1692–1695.

19. K. Ladomenou, T. N. Kitsopoulos, G. D. Sharma, A. G. Coutsolelos, The importance of various anchoring groups attached on porphyrins as potential dyes for DSSC Applications, RSC Adv. 4 (2014) 21379.

20. L. Zhang, J. M. Cole, Anchoring Groups for Dye-Sensitized Solar Cells, ACS Appl. Mater. Interfaces 7 (2015) 3427–3455.

21. B. J. Brennan, z M. J. Llansola Portole´s, P. A. Liddell, T. A. Moore, A. L. Moore, D. Gust, Comparison of silatrane, phosphonic acid, and carboxylic acid functional groups for attachment of porphyrin sensitizers to TiO_2 in photoelectrochemical cells, Phys. Chem. Chem. Phys. 15 (2013) 16605-16614.

22. W. M. Campbell, A. K. Burrell, ,D. L. Officer, K. W. Jolley, Porphyrins as light harvesters in the dye-sensitised TiO_2 solar cell, Coordination Chemistry Reviews 248 (2004) 1363–1379.

23. K. Hanson, M. K. Brennaman, H. Luo, C. R. K. Glasson, J. J. Concepcion, W. Song, T. J. Meyer, Photostability of Phosphonate-Derivatized, Ru^{II} Polypyridyl Complexes on Metal Oxide Surfaces, ACS Appli. Materials and Intefaces. 4, (2012), 1462.

24. D. G. Brown, P. A. Schauer, J. B. Garcia, B. R. Fancy, C. P. Berlinguette, Stabilization of Ruthenium Sensitizers to TiO_2 Surfaces through Cooperative Anchoring Groups, J. Am. Chem. Soc. 135 (2013) 1692−1695.

25. K. Kenji, Y. Masak , F. Emi, K. Toru, U. Masafumi, H. Minoru, High Performance of Si–O–Ti Bonds for Anchoring Sensitizing Dyes on TiO_2 Electrodes in Dye sensitized Solar Cells Evidenced by Using Alkoxysilylazobenzenes, Chem. Lett. 39 (2010) 260-262.

26. M. J. Frisch, G. W. Trucks, H. B. Schlegel, G. E. Scuseria, M. A. Robb, J. R. Cheeseman, G. Scalmani, V. Barone, B. Mennucci, G. A. Petersson, H. Nakatsuji, M. Caricato, X. Li, H. P. Hratchian, A. F. Izmaylov, J. Bloino, G. Zheng, J. L. Sonnenberg, M. Hada, M. Ehara, K. Toyota, R. Fukuda, J. Hasegawa, M. Ishida, T. Nakajima, Y. Honda, O. Kitao, H. Nakai, T. Vreven, J. A. Montgomery, Jr., J. E. Peralta, F. Ogliaro, M. Bearpark, J. J. Heyd, E. Brothers, K. N. Kudin, V. N. Staroverov, R. Kobayashi, J. Normand, K. Raghavachari, A. Rendell, J. C. Burant, S. S. Iyengar, J. Tomasi, M. Cossi, N. Rega, J. M. Millam, M. Klene, J. E. Knox, J. B. Cross, V. Bakken, C. Adamo, J. Jaramillo, R. Gomperts, R. E. Stratmann, O. Yazyev, A. J. Austin, R. Cammi, C. Pomelli, J. W. Ochterski, R. L. Martin, K. Morokuma, V. G. Zakrzewski, G. A. Voth, P. Salvador, J. J. Dannenberg, S. Dapprich, A. D. Daniels, O. Farkas, J. B. Foresman, J. V. Ortiz, J. Cioslowski, D. J. Fox, Gaussian 09, Revision A.02, Gaussian, Inc., Wallingford CT, 2009..

27. A. Pradhan, T. Morimoto, M. Saikiran, G. Kapil, S. Hayase, S. S. Pandey, Investigation of minimum driving force for the dye regeneration utilizing model squaraine dyes for dye-sensitized solar cells, J. Mater. Chem. A 5 (2017) 22672-22682

28. M. Saikiran, D. Sato, S. S. Pandey, T. Ohta, S. Hayase, T. Kato, Photophysical characterization and BSA interaction of the direct ring carboxy functionalized unsymmetrical NIR cyanine dyes, Dyes and Pigments 140 (2017) 6-13.

29. J. W. Park, Y. S. Kim, K. J. Lee, D. J. Kim, Novel Cyanine Dyes with Vinylsulfone Group for Labeling Biomolecules, Bioconjugate Chem. 23 (2012) 350-362.

30. S. A. Archer, T. Keane, M. Delor, E. Bevon, A. J. Auty, D. Chekulaev, I. V. Sazanovich, M. Towrie, A.J. H. M. Meijer, J. A. Weinstein, Directly Coupled Versus Spectator Linkers on Diimine PtII Acetylides—Change the Structure, Keep the Function?, Chem. Eur. J. 23 (2017) 8239–18251.

31. A. Anthonysamy, Y. Lee, B. Karunagaran, V. Ganapathy S.W. Rhee, S. Karthikeyan, K. S. Kim, M. J. Ko, N.-G. Park, M.-J. Ju, J. K. Kim, Molecular design and synthesis of ruthenium (II) sensitizers for highly efficient dye-sensitized solar cells, Journal of Materials Chemistry 21 (2011) 12389-12397.

32. S. Sreejith, P. Carol, P. Chithraa, A. Ajayaghosh, Squaraine dyes: a mine of molecular materials, J. Mater. Chem. 18 (2008) 264-274.

33. Lim JM, Yoon ZS, Shin JY, Kim KS, Yoon MC, Kim D., The photophysical properties of expanded porphyrins: relationships between aromaticity, molecular geometry and non-linear optical properties, Chem Commun (Camb). 3 (2009) 261-73.

34. T. Geiger, S. Kuster, J.H. Yum, S.J. Moon, M. K. Nazeeruddin, M. Grätzel, F. Nuësch, Molecular Design of Unsymmetrical Squaraine Dyes for High Efficiency Conversion of Low Energy Photons into Electrons Using TiO_2 Nanocrystalline Films, Adv. Funct. Mater. 19 (2009) 2720–2727

35. B. Su, H. H. Girault, Absolute Standard Redox Potential of Monolayer-Protected Gold Nanoclusters, J. Phys. Chem. B 109 (2005) 11427-11431.

36. Y Ogomi, T Kato, S Hayase, Dye Sensitized Solar Cells Consisting of Ionic Liquid and Solidification, Journal of Photopolymer Science and Technology 19 (2006) 403-408.

37. M.K. Nazeeruddin, F.D. Angelis, S. Fantacci, A. Selloni, G. Viscardi, P. Liska, S. Ito, B. Takeru, M. Grätzel, Combined experimental and DFT-TDDFT computational study of photo electrochemical cell ruthenium sensitizers, J Am Chem Soc. 127 (2005) 16835-16847.

38. S.S. Pandey, T. Morimoto, N. Fujikawa, S. Hayase, Combined theoretical and experimental approaches for development of squaraine dyes with small energy barrier for electron injection, Solar Energy Materials and Solar Cells 159 (2017) 625-632.

39. A. Baktash, B. Khoshnevisan, A. Sasani, K. Mirabbaszadeh, Effects of carboxylic acid and phosphonic acid anchoring groups on the efficiency of dye sensitized solar cells: A computational study, Organic Electronics 33 (2016) 207-212.

40. T. N. Murakami, E. Yoshida, N. Koumura, Carbazole dye with phosphonic acid anchoring groups for long-term heat stability of dye-sensitized solar cells, Electrochimica Acta 131 (2014) 174-183.

41. H. Park, E. Bae, J. J. Lee, J. Park, W. Choi, Effect of the Anchoring Group in Ru−Bipyridyl Sensitizers on the Photoelectrochemical Behavior of Dye-Sensitized TiO_2 Electrodes: Carboxylate versus Phosphonate Linkages, J. Phys. Chem. B 110 (2006) 8740-8749.

42. V. Johansson, L. E. Gibbings, T. Clarke, M. Gorlov, G.G. Andersson, L. Kloo, On the correlation between dye coverage and photo electrochemical performance in dye-sensitized solar cells, Physical Chemistry Chemical Physics 16 (2014) 711-718.

43. A. C. Khazraji, S. Hotchandani, S. Das, P. V. Kamat, Controlling Dye (Merocyanine-540) Aggregation on Nanostructured TiO_2 Films. An Organized Assembly Approach for Enhancing the Efficiency of Photosensitization, J. Phys. Chem. B 103 (1999) 4693-4700.

44. Md. K. Nazeeruddin, R. H. Baker, P. Liska, M. Grätzel, Investigation of Sensitizer Adsorption and the Influence of Protons on Current and Voltage of a Dye-Sensitized Nanocrystalline TiO_2 Solar Cell, J. Phys. Chem. B 107 (2003) 8981-8987.

45. Y. Ogomi, S.S. Pandey, S. Kimura, S. Hayase, Probing mechanism of dye double layer formation from dye-cocktail solution for dye-sensitized solar cells, Thin Solid Films 519 (2010) 1087-1092.

46. M. Kawano, T. Nishiyama, Y. Ogomi, S.S. Pandey, T. Ma, S. Hayase, Relationship between diffusion of Co^{3+}/Co^{2+} redox species in nanopores of porous Titania stained with dye molecules, dye molecular structures, and photovoltaic performances, RSC Advances 5 (2015) 83725-83731.

47. J. H. Yum, S. J. Moon, R. H.-Baker, P. Walter, T. Geiger, F. Nüesch, M Grätzel, Md. Nazeeruddin, Effect of coadsorbent on the photovoltaic performance of squaraine sensitized nanocrystalline solar cells, Nanotechnology 19 (2008) 1-6.

48. G. M. Shivashimpi, S. S. Pandey, A. Hayat, N. Fujikawa, Y. Ogomi, Y. Yamaguchi, S. Hayase. Far-red sensitizing octatrifluorobutoxy phosphorous triazatetrabenzocorrole: Synthesis, spectral characterization and aggregation studies, Journal of Photochemistry and Photobiology A: Chemistry 289 (2014) 53–59.

49. Y. S. Kim, K. Liang, K. Y. Law, D. G. Whitten, An investigation of photocurrent generation by squaraine aggregates in monolayer-modified tin oxide (SnO_2) electrodes, J. Phys. Chem. 98 (1994) 984–988.

50. T. Inoue, S. S. Pandey, N. Fujikawa, Y. Yamaguchi, S. Hayase, Synthesis and characterization of squaric acid based NIR dyes for their application towards dye-sensitized solar cells, Journal of Photochemistry and Photobiology A: Chemistry 213 (2010) 23–29.

51. R. G. Franz, Comparisons of pKa and log P values of some carboxylic and phosphonic acids: Synthesis and measurement, AAPS PharmSci 3 (2001) 1-13.

Figure Captions:

Figure 1. Chemical structure of the unsymmetrical squaraine dyes with varying anchoring groups.

Figure 2. Synthetic scheme for the preparation of unsymmetrical squaraine dyes bearing different anchoring groups. (A) 1-Iodododecane, Propionitrile, Reflux/ 26 hrs. (B) 3, 4-Diethoxy-3-cyclobutene-1, 2-dione, Triethylamine, Ethanol, Reflux/15 hrs. (C) 4N NaOH, Ethanol, Reflux/2 hrs. (D) n-Butanol: Toluene (1:1). (E) TMSBr, DCM, RT.

Figure 3. Electronic absorption (solid line) and fluorescence emission (dotted line) spectra of unsymmetrical squaraine dyes in ethanol solution.

Figure 4. CV of the unsymmetrical squaraine dyes and ferrocene in DMF recorded at 50 mV/s scan rate using Pt working/counter electrode and saturated calomel electrode (SCE) as reference electrode.

Figure 5. Energy band diagram for the unsymmetrical squaraine dyes under investigation. Values shown in the parentheses are theoretically calculated values by TD-DFT using 6-311G/B3PW91.

Figure 6. Theoretically calculated electron density distribution in the HOMO (bottom) and LUMO (top) for the unsymmetrical squaraine dyes bearing different anchoring groups.

Figure 7. Normalized solid-state absorption spectra of squaraine dyes adsorbed on mesoporous TiO_2 (a) and kinetics of dye adsorption by monitoring the absorbance at the λ_{max} of respective dyes for different time intervals (b).

Figure 8. Photovoltaic characteristics of the DSSCs fabricated using unsymmetrical squaraine dyes bearing different anchoring groups.

Figure 9. Photovoltaic characteristics of the DSSCs fabricated using unsymmetrical squaraine dyes bearing different anchoring groups for a fixed dye density of about 20 nmol/cm2 in their respective photoanodes.

Figure 10. Photovoltaic stability of the DSSCs under continuous 1 Sun light (100 mW/cm^2) irradiation fabricated using unsymmetrical squaraine dyes bearing different anchoring groups.

Figure 11. Normalized PCE of the DSSCs after simulated solar irradiation of 100 mW/cm^2 using unsymmetrical squaraine dyes with different anchoring groups. After device fabrication, DSSCs were stored at room temperature and photovoltaic performance was evaluated after different time intervals for a period of two weeks. Arrow indicates the day on which, electrolyte was re-filled.

Table 1. Optical parameters for unsymmetrical squaraine dyes in ethanol solution and thin film adsorbed on TiO$_2$.

Dye	ε (dm^3. Mol^{-1}.cm^{-1})	Absorption (solution) λ_{max}	Emission (solution) λ_{max}	Stokes Shift	Absorption (TiO$_2$) λ_{max}	Optical absorption edge (eV)
SQ-138	3.1 x 10^5	654 nm	668 nm	14 nm	654 nm	710 nm (1.75 eV)
SQ-141	2.4 x 10^5	660 nm	674 nm	14 nm	670 nm	725 nm (1.71 eV)
SQ-142	1.8 x 10^5	652 nm	660 nm	8 nm	652 nm	700 nm (1.77 eV)
SQ-143	4.8×10^5	652 nm	664 nm	12 nm	656 nm	710 nm (1.75 eV)

Table-2 Dye desorption behavior and anchoring stability of unsymmetrical squaraine dyes on the mesoporous TiO_2.

Dye	Dye desorption after 3 hours (nmol/cm^2) [% Removal]	Total dye loading (nmol/cm^2)	Rate of dye desorption (% dye/ min.)
SQ-138	23.37 [76.7 %]	30.48	0.426
SQ-141	2.97 [47.5 %]	6.25	0.263
SQ-142	18.13 [99.3 %]	18.24	0.551
SQ-143	2.56 [1.1 %]	228.70	0.006

Table 3. Photovoltaic parameters of DSSCs fabricated using unsymmetrical squaraine dyes after simulated solar irradiation.

Dye sensitizers	Anchoring group	Jsc (mA/cm^2)	Voc (V)	FF	Efficiency (%)
SQ-138	-COOH	12.49	0.60	0.53	4.07
SQ-141	-OH	1.96	0.52	0.61	0.63
SQ-142	-SO$_3$H	6.13	0.62	0.59	2.28
SQ-143	-PO$_3$H$_2$	3.39	0.54	0.55	1.02

Table 4. Photovoltaic parameters of DSSCs fabricated using unsymmetrical squaraine dyes with fixed dye loading of about 20 nmol/cm^2 in the respective photoanodes.

Dye sensitizers	Anchoring group	Jsc (mA/cm^2)	Voc (V)	FF	Efficiency (%)
SQ-138	-COOH	5.87	0.61	0.62	2.25
SQ-141	-OH	2.32	0.59	0.67	0.92
SQ-142	-SO$_3$H	5.11	0.60	0.66	2.05
SQ-143	-PO$_3$H$_2$	1.66	0.58	0.64	0.62
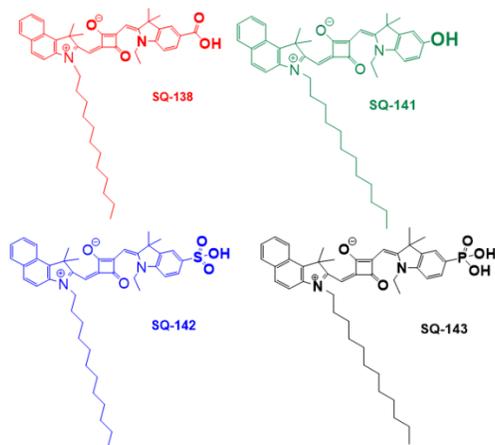
Figure 1
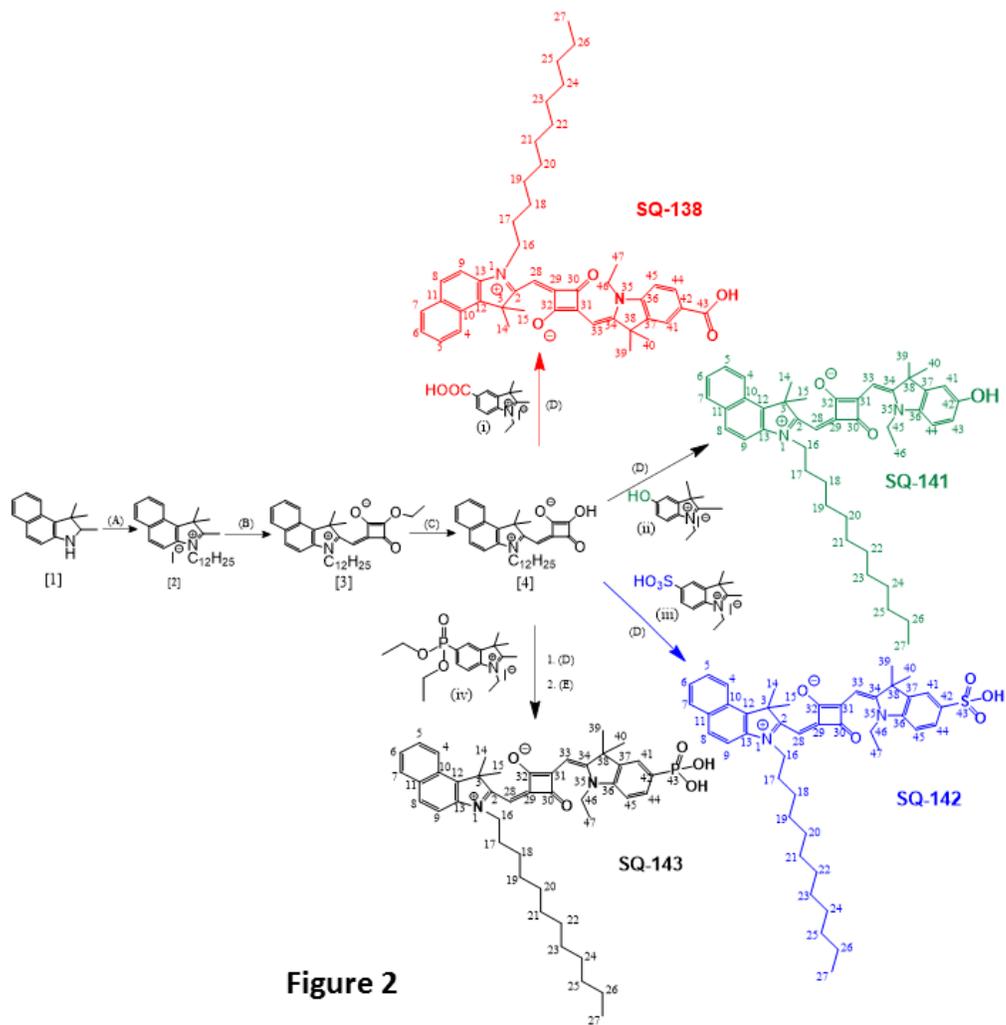
Figure 2
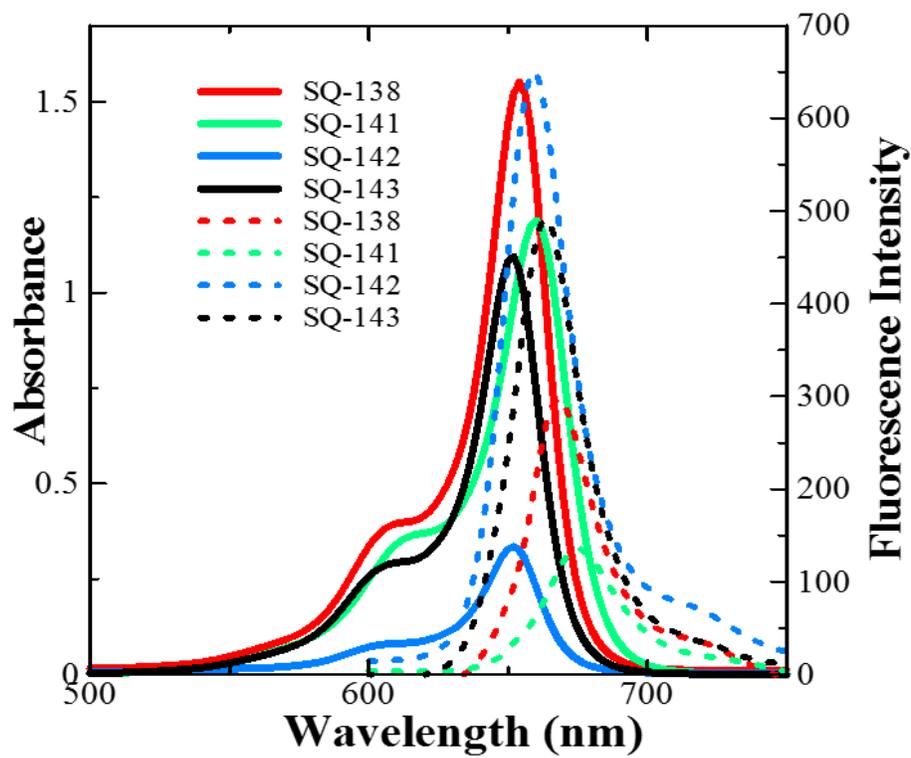
Figure 3

Figure 4

Figure 5

(SQ-138)　　(SQ-141)　　(SQ-142)　　(SQ-143)
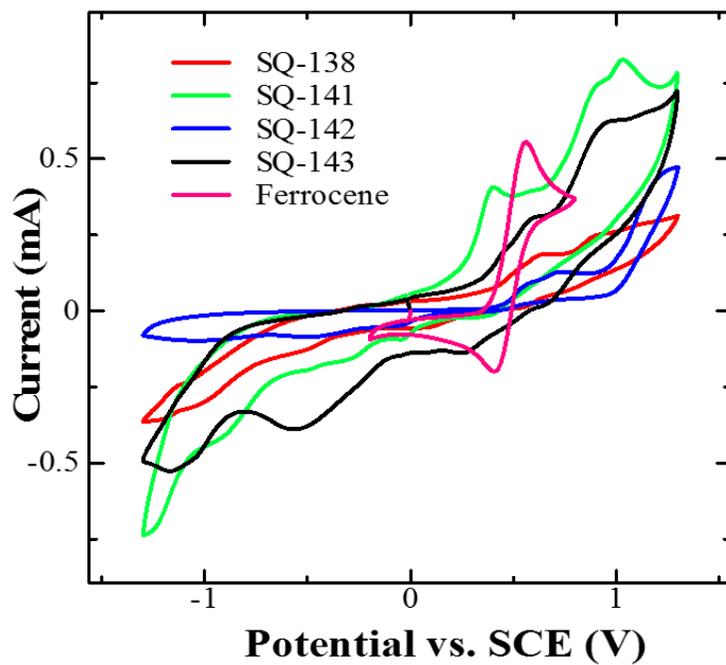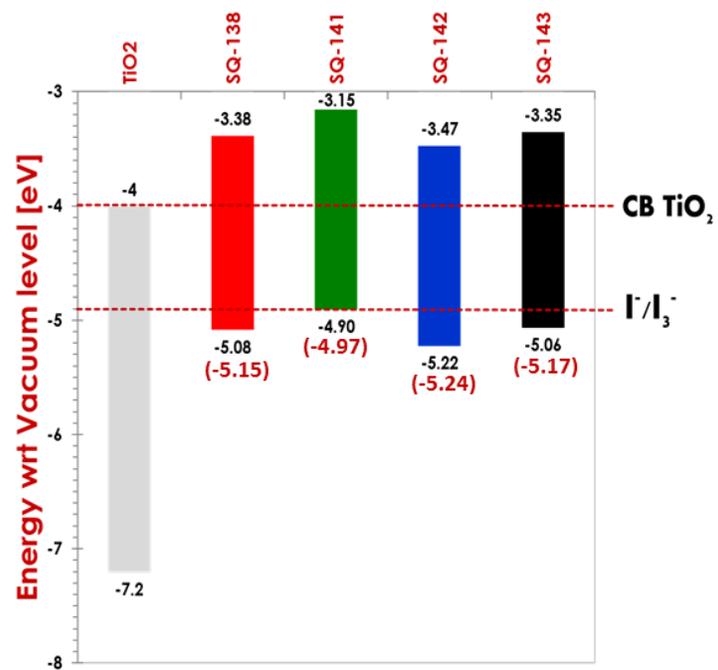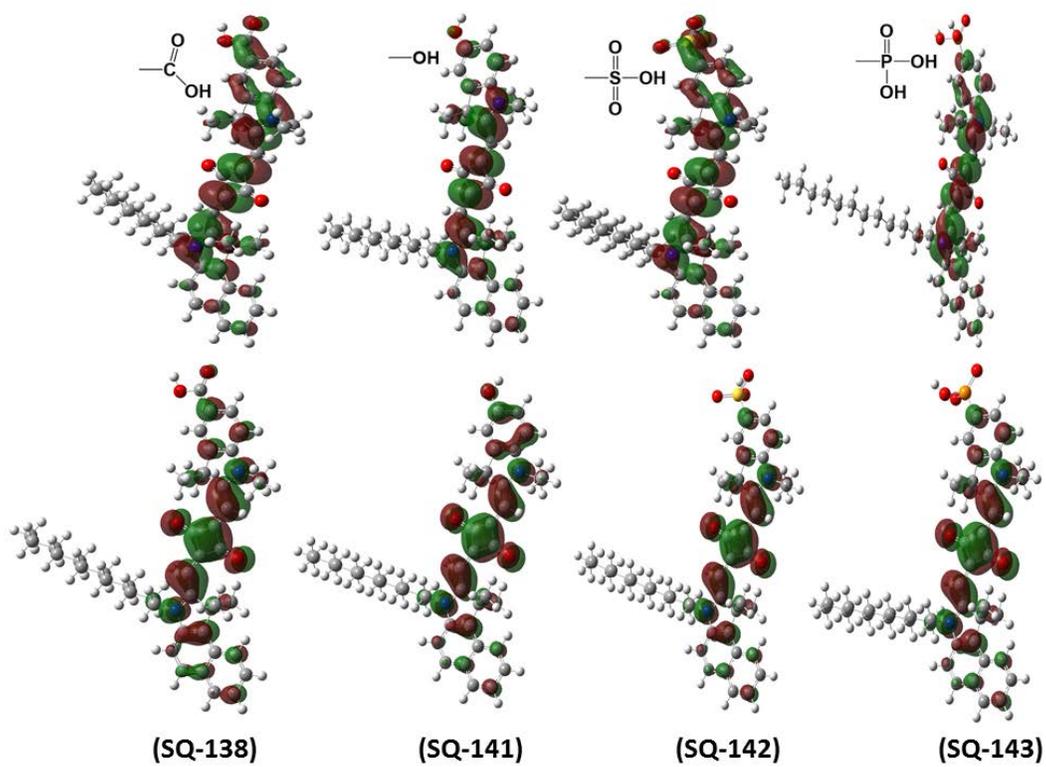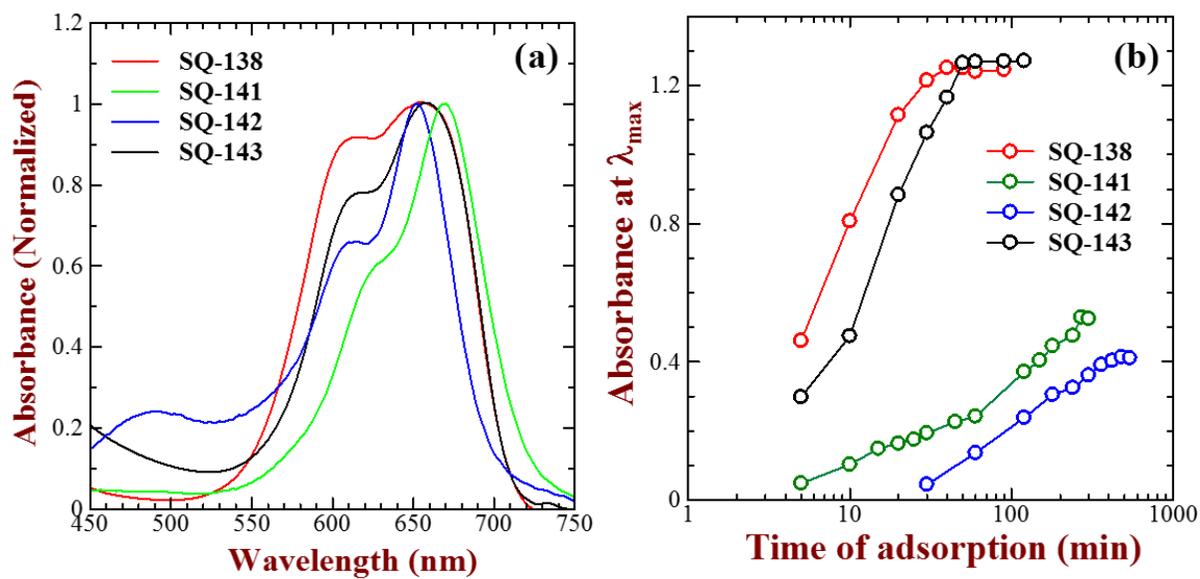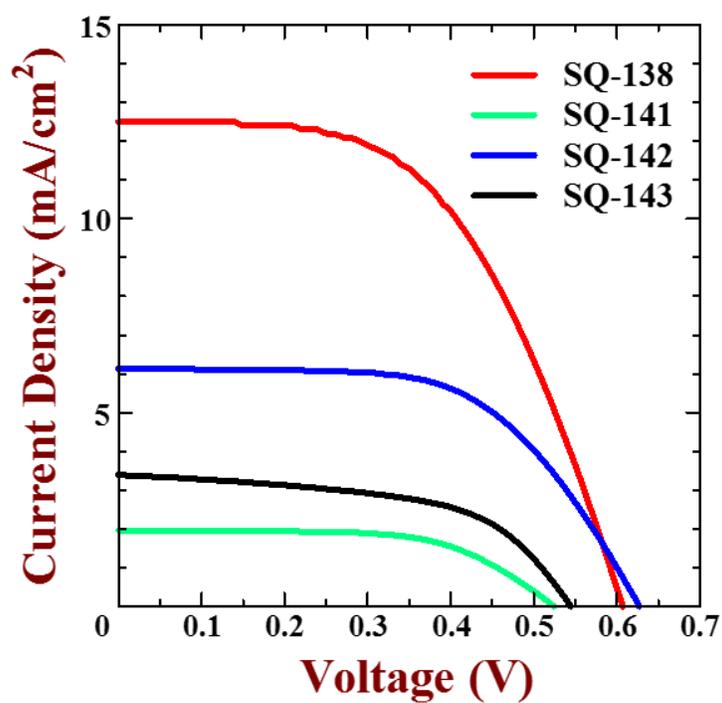
Figure 6

Figure 7

Figure 8
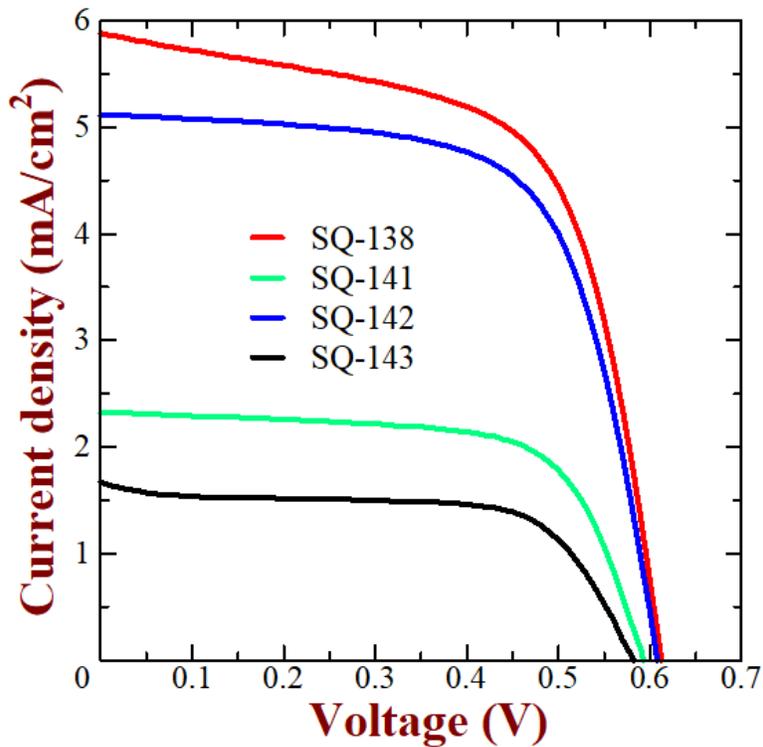
Figure 9

Figure 10

Figure 11